VLT OPTICAL AND NEAR-IR OBSERVATIONS OF THE Z=6.28 QUASAR SDSS 1030+0524

Laura Pentericci[2], Xiaohui Fan[3], Hans Walter Rix[2], Michael A. Strauss[4], Vijay K. Narayanan[4], Gordon T. Richards[5], Donald P. Schneider[5], Julian Krolik[6], Tim Heckman[6], Jonathan Brinkmann[7], Don Q. Lamb[8], Gyula P. Szokoly[9]
Submitted to the Astronomical Journal

ABSTRACT

We present new VLT spectroscopic observations of the most distant quasar known, SDSS J1030+0524 at z=6.28, which was recently discovered by the Sloan Digital Sky Survey. We confirm the presence of a complete Gunn-Peterson trough caused by neutral hydrogen in the intergalactic medium. There is no detectable flux over the wavelength range from 8450 to 8710 Å. We set a stronger limit on the drop of the flux level blueward of the Lyα line: a factor of > 200. Below 8450 Å the spectrum shows a rise in flux, with a large fraction (> 60 %) of the total emission produced by few narrow features of transmitted flux. We discuss the proximity effect around this quasar, with the presence of transmitted flux with many absorption features in a region of about $23h^{-1}$ comoving Mpc. If assuming the surrounding medium were completely neutral, the size of this region would imply a quasar lifetime of $\sim 1.3 \times 10^7$ years.

We also present near-IR spectroscopy of both SDSS J1030+0524 and of SDSS J1306+05, the second most distant quasar known, at redshift 6.0. We combine measurements of the CIV line and limits on the HeII emission from the near-IR spectra with the NV line measurements from the optical spectra to derive the metal abundances of these early quasar environments. The results are indistinguishable from those of lower redshift quasars and indicate little or no evolution in the metal abundances from z$\sim$ 6 to z$\sim$2. The line ratios suggest supersolar metallicities, implying that the first stars around the quasars must have formed at least a few hundreds of Myrs prior to the observation, i.e., at redshifts higher than 8.

Subject headings: cosmology: observations — galaxies: formation — galaxies: quasars: absorption lines — galaxies: quasars: individual (SDSS 1030+0524, SDSS 1306+0356)

1. INTRODUCTION

Quasars are amongst the most luminous objects in the Universe, allowing us to study them and any intervening material out to very large distances, corresponding to lookback times when the Universe was very young. Hence finding and studying quasars at high redshifts is one of the best ways to constrain the physical conditions in the early Universe. The mere existence of luminous quasars at such early times, and the implied presence of black holes with M $\geq 10^9$ M$_\odot$ place stringent limits on the epoch at which massive condensed structures formed, thereby constraining structure formation models (e.g. Efstathiou and Rees 1988). At high redshifts such luminous quasars must be associated with very massive halos, hence they are expected to be found near high peaks (4-5 σ or more) of the large scale density field (e.g. Efstathiou & Rees 1988, Nusser & Silk 1993) that collapsed sufficiently early. Furthermore, several arguments suggest that the formation of elliptical galaxies and massive bulges are paralleled by an early quasar phase (e.g. Kauffmann & Haehnelt 2000).

The spectra of high redshift quasars contain important information on the enrichment history of the gas in the quasar environment, and probe the star formation preceding the epoch at which the quasars are observed, possibly the first stars that formed in massive collapsed structures (e.g. Hamann & Ferland 1999). Finally, high redshift quasars serve as probes of the intergalactic medium via the absorption of the Lyman α forest.

The Sloan Digital Sky Survey (SDSS – York et al. 2000) has, amongst its scientific aims, the construction of the largest sample of quasars ever, with more than 10^5 objects spanning a large range of redshift and luminosities. The SDSS has already found an unprecedented number of new high redshift quasars, including more than 200 new quasars at z$\geq$4 (e.g. Fan et al. 2000, Zheng et al. 2000, Anderson et al. 2001, Fan et al. 2001a, Schneider et al. 2001). These high redshift quasars have been efficiently selected by their distinctive position in color-color diagrams, with characteristic colors due to the main feature of the quasar spectra, viz., the strong Lyα emission line, the Lyα forest and the Lyman limit.

Recently, Fan et al. (2001b) presented the discovery of SDSS J1030+0524, found during follow-up spectroscopy of i-band drop-out objects, i.e. objects showing very red $i^* - z^*$ color and relatively blue z^*-J colors (following the notation of previous SDSS papers, we use the superscript * for the photometry, and the letters alone for the filters, Stoughton et al. 2002). Moderate signal to noise ratio (S/N) optical spectra taken with the ARC 3.5m telescope showed very strong (rest-frame equivalent width EW$\sim$50 Å) Lyα + NV emission at $\sim$8850 Å and $\sim$9050 Å, respectively. Based on a fit of the CIV line the redshift was estimated estimated to be z$\sim$ 6.28 which makes it unambiguously the most distant quasar known. Follow up optical spectroscopic observations with Keck (Becker et al. 2001) have shown the first clear detection of a complete Gunn-Peterson trough (Shklovsky 1964, Scheuer 1965, Gunn & Peterson 1965) in the spectrum of this quasar. The flux level drops by a factor of at least 140 relative to an estimate of the unabsorbed continuum level, and the spectrum is consistent with zero flux in the Lyα forest region immediately blueward of the Lyα emission line. Even if the existence of the trough itself does not imply that the quasar is observed prior to the re-ionization epoch (e.g. Barkana 2001), the fast evolution of the mean absorption in the spectra of quasars at z$>$ 5 suggests that the universe is approaching the reionization epoch at z$\sim$ 6 (Becker et al. 2001, Fan et al. 2001b, Djorgovski et al. 2001). In a companion paper (Fan et al. 2001c), we use cosmological simulations to estimate the evolution of the ionizing background and to constrain the redshift of reionization (see also Gnedin 2000, Cen & McDonald 2001, Lidz et al. 2001).

We have obtained an optical VLT spectrum of the quasar to independently measure the Gunn-Peterson trough and to set tighter limits on the transmitted flux. We have also obtained a near-IR spectrum, to set constraints on the metallicity of the quasar environment and to better estimate the redshift from the CIV emission line, which unlike Lyα is not affected by intervening absorption. Finally we obtained a near-IR VLT spectrum of the second most distant quasar SDSS J1306+0356 at z=5.99 (Fan et al. 2001b). We will use the results from this spectrum in the discussion of the metallicity in high redshift quasars.

The paper is organized as follows: in Section 2 we describe the observations and present the optical and near-IR spectra of the two quasars. In Section 3 we discuss the main results obtained from the optical spectrum: the Gunn-Peterson trough and the limits we can set from the new data, as well as the region in which flux is present, and the proximity effect. In Section 4 we derive the metallicity in the two highest redshift quasars and discuss its implication for the star formation timescales.

Throughout the paper we assume a flat, Λ-dominated universe with $H_0 = 65$ km s^{-1} Mpc^{-1}, $\Lambda = 0.65$ and $\Omega = 0.35$ (Ostriker & Steinhardt 1995; Krauss & Turner 1995).

2. OBSERVATIONS AND RESULTS

2.1. *Optical spectroscopy*

Optical long slit spectroscopic observations were carried out in service mode on 28 and 30th of June 2001, with the FORS2 spectrograph mounted on VLT/YEPUN on Paranal. On each night, the quasar SDSS 1030+0524 was observed for a total of 3600 sec divided into two 30 minute exposures. The target was placed at different locations along the slit for each individual frame, to minimize problems related to flat fielding and other possible systematic errors. Weather conditions were clear but not photometric. The seeing was of order 0.8$''$ on both nights. We used a 1$''$ slit together with the new holographic grism GRISM_1028z+29 and the order separation filter OG590, which has greatest sensitivity at $\lambda \approx 8800$Å, and covers the wavelength range we are interested in (7900 Å to 9300 Å) This grism also offers the highest resolving power, R$\sim$ 2700, corresponding to a resolution of ~ 3.1 Å, which will allow us to cleanly resolve out the night sky, thereby significantly increasing our signal-to-noise ratio and our ability to subtract the sky. The dispersion of the spectrum is 0.68 Å per pixel. Given the rather high airmass of $1.4 < \sec(z) < 1.9$ for the observations, the slit was kept at the parallactic angle.

Image reduction (including bias subtraction, flat fielding and correction for slit distortion for each individual frame) was performed with standard IRAF procedures. The most critical part of the reduction was the sky-background subtraction, especially due to the presence of strong sky emission lines in the wavelength region where the flux is very close to zero. In particular the absolute level of flux detection changes slightly (by $\sim 1\sigma$) depending on the parameters used for sky subtraction. We therefore assumed that outside the trace of the spectrum of the quasar, i.e. at other places along the slit, there was no flux. Therefore after the normal sky subtraction, we determined the average of the residual sky signal in a large region on either side of the spectrum and subtracted this single value from the entire data frame.

Wavelength calibration was done using observations of a Xe-Ar lamp obtained during the morning calibration: the intrinsic accuracy of the wavelength fit is better than 0.2 Å. To this error we have to add the uncertainty due to the large range of airmasses of the observations, which we estimate from the spectra as less than half a pixel. The total uncertainty is then 0.4 Å. Relative flux calibration was performed using a long slit spectrum taken with the same setup of the spectrophotometric standard EG274 (Hamuy et al. 1992). The spectra from each night were calibrated separately and then coadded using a cosmic-ray rejection algorithm. Finally the spectrum was extracted: since we could not trace it from the image itself, due to the absence of intrinsic quasar flux throughout the Gunn-Peterson trough (see below), we used the trace derived from the standard star. The spectrum was not corrected for telluric absorption. The two-dimensional spectrum and the extracted one-dimensional spectrum (smoothed to 3 Åper pixel) are presented in Figure 1. The main characteristics of the Lyα and NV emission lines are given in Table 1.

2.2. *Near-IR Spectroscopy*

Near-IR observations of SDSS 1030+0524 were carried out in service mode with ISAAC on VLT-ANTU on 18 May 2001. Observations were made with the SW Rockwell 1024×1024 pixel Hawaii array which has a scale of 0.148 arcsec/pixel and the lower resolution grating, whose resolving power with a 0.6$''$ slit is 860. The seeing dur-

ing the night varied between 0.4 " and 0.7". The total integration time was 5760 sec, split into 2 sets of 16 images. We used a detector integration time DIT=180 sec over which time a single integration was done (NDIT=1). The object was moved between exposures by 20″ along the slit in a ABBA sequence, with an extra jitter of amplitude 5-10″ around each A and B position. The airmass varied between 1.15 and 1.27.

The ISAAC data were reduced in the standard way with IRAF, subtracting each image from its adjacent one. After flat fielding, we corrected each frame for geometric distortions using the sky lines as well as a spectrum of an argon lamp, which also led to wavelength calibration. Finally the frames were aligned using the shifts from the image headers and combined with the IRAF/avsigclip rejection algorithm. The spectrum was then extracted using a 3 pixel aperture, with a trace derived from the spectrum itself. Unfortunately the telluric star from the ESO standard calibration plan was observed with a different instrument configuration. Since no telluric spectra were present in the ESO database, the observations were repeated on the 15th of June with a seeing of around 0.5″ and at similar airmass as the science observations. The standard telluric star (H 78530) was reduced in a similar way as the spectrum, and in particular the wavelength calibration was done with a lamp exposure taken on the same night. However, it is apparent that the removal of telluric features from our data is not perfect and the resulting spectrum is noisier than we had hoped. Finally the spectrum was flux calibrated using the total J band magnitude of the object (J=18.87± 0.10, Fan et al. 2001b) and is presented in Figure 2. The measured characteristics of the CIV line and the 3σ limits on the undetected HeII line are reported in Table 1. Contrary to what we hoped, the redshift we derive from the CIV line is actually less accurate than that derived from the lines in the optical spectrum: the reason is the uncertainty in the removal of some deep telluric features at the same wavelength as the CIV emission line.

An infrared spectrum of the quasar SDSS J1306+0356 at z=5.99 was obtained with ISAAC with the aim of detecting the CIV line. The observations were carried out in service mode on 1 July 2001; the total integration time was 5760 sec, which was divided into 2 sets of 16 images, each with 180 sec integration time. We used the SZ filter, which gives a total wavelength coverage from 0.98 μm to 1.14μm. The airmass during the observations varied from 1.19 to 1.39 and the typical seeing was 0.8″. The observational strategy was the same as for SDSS 1030+0524. Reduction was carried out as described above. The telluric features were eliminated with observation of the telluric standard H74113 , observed with the same set-up of the target during the same night. The resulting spectrum is shown in Figure 3. The two absorption features at $\lambda \sim$9900 Å that are observed in the spectrum are due to MgII absorption at redshifts 2.20 and 2.53, respectively. No obvious intergalactic CIV absorption is seen.

From a fit to the peak of the CIV line we derive a redshift of 6.00±0.01 for this quasar, consistent with the z_{em}=5.99±0.02 derived by Becker et al. (2001) from optical emission lines (NV). Note that the CIV line is often offset relative to the systemic quasar redshift, e.g. for

z∼ 2 SDSS quasars Richards et al. (2002) find an average shift between the CIV line and the systemic redshift on the order of 800 km/s, with some shifts as large as 3000 km/s (see also Vanden Berk et al. 2001, Laor et al. 1995). However in our case the CIV redshift agrees within the errors with the redshift derived by NV which is normally very close to the systemic redshift, so we believe there are no such extreme offsets; in the error quoted above we have included a possible uncertainty of 500 km/s. The profile of the CIV line actually suggests the presence of both broad and narrow components; fitting the overall shape with two gaussians gives FWHM for the two components of 1600±200 km/s and 4400±400 km/s respectively; the broad component is blueshifted relative to the narrow one. No limits can be derived for the undetected HeII line since it falls at the edge of the spectrum where the S/N is very low.

3. RESULTS

3.1. *The Gunn-Peterson trough: the limits from the VLT spectrum*

In the bottom panel of Figure 1, we show the two-dimensional spectrum of SDSS 1030+0524 in the wavelength region between 7990 Å and 9250 Å. Clearly there is a sharp drop in flux, blueward of the Lyα emission, and the flux is consistent with zero in the region between 8450 Å and 8710 Å.

Following previous papers (e.g. Fan et al. 2001b) we have computed the transmitted flux ratio over 3 small redshift windows in z_{abs} as $T(z_{abs}) = \langle f_\nu^{obs}/f_\nu^{con} \rangle$, where f_ν^{obs} is the observed flux and f_ν^{cont} is the intrinsic quasar continuum flux. For the latter quantity we have assumed a power law, with $f_\nu^{con} \propto f_\nu^{-0.5}$ (or $f_\nu^{con} \propto f_\lambda^{-1.5}$). We normalized this to the continuum flux measured at an observed wavelength of 9200 Å(with the normalization value $f_\lambda = 1 \times 10^{-17}$ erg s^{-1} cm^{-2} Å^{-1}), since this is the only range of our optical spectrum free from emission and absorption lines.

The average flux ratio in the three wavelength bins is 0.046± 0.005, 0.029± 0.004 and 0.001 ± 0.004 respectively in the intervals 8000-8200 Å, 8200-8450 Å and 8450-8710 Å, approximately corresponding to z_{abs} of 5.65, 5.85 and 6.05. The error bars include only the photon noise, and do not reflect the systematic error due to the unknown continuum shape (which however should be smaller, as argued by Fan et al. 2001b). The results are consistent with those reported by Becker et al. (2001) from the Keck spectroscopic observations. Therefore, we confirm the non-detection of flux found in Keck spectrum in the same wavelength range. We emphasize that these are completely independent measurements, using a different telescope at a different site with a different instrument, and both spectra show the same non-detection of flux.

The implied drop of flux for the wavelength region 8450-8710 Å is a factor of 200 at a 1σ level, a stronger limit than previously reported by Becker et al. (2001), who derived a factor of 140, also at 1σ. The corresponding effective Gunn-Peterson optical depth, $\tau_{eff} \equiv -\ln(T)$, is > 5.3. Note that we cannot compute the D$_A$ parameter defined in Oke & Korycansky (1982) as D$_A \equiv \langle 1 - f_\nu^{obs}/f_\nu^{con} \rangle$ measured in the region between restframe Lyα and Lyβ (λ=1050 and 1170 Å) and is normally used to describe the
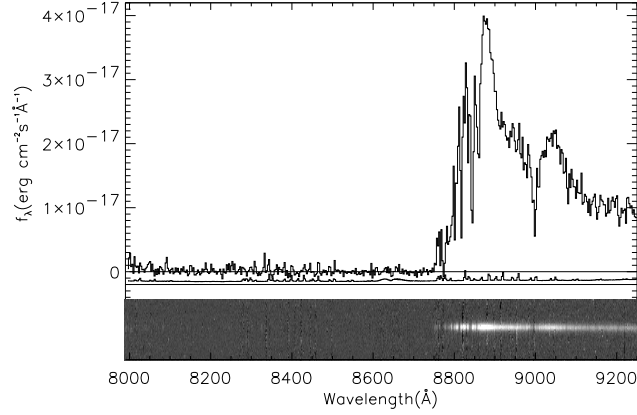
FIG. 1.— Upper panel: the VLT/FORS2 one-dimensional optical spectrum of the quasar SDSS 1030+0524 shown in the observed frame and smoothed to a dispersion of 3 Å pixel^{-1}. The bottom line shows the error array derived from the sky spectrum and offset by -0.2×10^{-17} cgs for clarity. Lower panel: a grey-scale representation of the sky-subtracted two-dimensional spectrum plotted on the same wavelength scale. The spatial extent of the plot is 40 pixels, corresponding to 20 arcseconds.
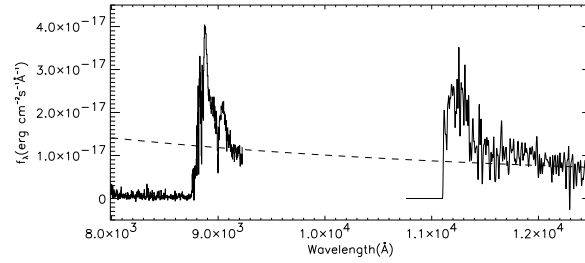

FIG. 2.— A composite of the optical and near IR (J band) spectra of SDSS 1030+0524. The dashed line is the continuum normalized at 12400 Å.
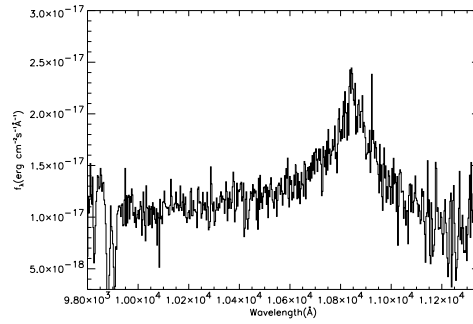

FIG. 3.— The z-band spectrum of the quasar SDSS 1306+0356, showing the CIV emission line.

decrement of flux below the Lyα line, because the wavelength range covered by our observations is not quite large enough.

The implication for the ionization state of the IGM are discussed in Fan et al. (2001c) where it is shown that the observed properties of the IGM at z∼6 are typical of those in the era at the end of the overlap stage of reionization when the individual HII regions merge. Thus this observation suggests that z∼6 marks the end of the reionization epoch.

3.2. *The spectrum below 8450 Å: IGM absorption between z=5.58 and 5.95*

The extracted spectrum shows some emerging flux below 8450 Å. However, from an inspection of the two-dimensional spectrum it appears that a large fraction of the flux comes from a few isolated transmission features, while the rest of the spectrum remains consistent with zero flux. In other words, a simple description of the transmitted flux in this region as arising from a uniform IGM is not sufficient. The presence of these gaps of transmitted flux can be explained, in the context of reionization, as due to cosmological HII regions around the sources that reionize the IGM before the epoch of overlap. The characteristics of these gaps, such as their sizes and probability distribution are important since they can put constraints e.g. on the nature of the ionizing sources (quasars and/or galaxies) on their lifetimes etc. In particular the reader is referred to Miralda-Escudé et al. (2000) for a detailed discussion of gaps in the Gunn-Peterson trough due to individual HII regions (see also Loeb & Barkana 2001, Djorgovski et al. 2001, Haiman & Loeb 1999).

In Figure 4 (left panel) we show the significance of any possible flux detection in the region between 8000 Å and 8750 Å: for each resolution element (the spectrum was binned to a resolution of 3 Å per pixel) the observed flux has been divided by its corresponding error array. There are no significant features ($> 3\sigma$) in the range between 8400-8750 Å, while there are several such features present in the shorter wavelength part of the spectrum. All the features above 3σ are also clearly recognized in the two-dimensional spectrum, and are visible on both spectra from the two different nights. We have tried to quantify what fraction of the total flux below 8400 Å is accounted for by these isolated features. To detect features in a systematic way, we used SEXtractor (Bertin & Arnouts 1996) on the two-dimensional sky-subtracted spectrum. We considered as an emission feature anything detected in more than 3 adjacent pixels with a flux larger than 1σ plus the local background as determined in an annulus around the feature. We considered only those features that have a peak of emission along the trace of the spectrum ($\pm$ 1 pixel); furthermore we eliminated all those features that were coincident with sky lines (by using the error array of the extracted spectrum), since these could be due to residuals of sky subtraction. This is a conservative approach since we might eliminate true features. Eight such features are detected from SEXtractor. We then measured the flux inside the features, assuming the width as given by SEXtractor in the dispersion direction, and 3 pixels in the spatial direction. The values measured are reported in Table 2, together with the central wavelength and the

width. The flux from these features accounts for 60% of the total flux in the 8000-8400 Å range.

To allow comparison with simulations, we also present the cumulative distribution of the transmitted flux ratio of the region between 8000 and 8450 Å (corresponding to a mean redshift of absorption z_{abs} =5.74) in Figure 4. For this plot the spectrum was rebinned to the resolution of 3 Å/pixel, and then divided by the assumed unabsorbed continuum flux estimated in the previous section. Ninety-nine per cent of the spectrum has a transmitted flux ratio less than 20% of the continuum, and the distribution goes to 100% very rapidly (note that all results depend on the resolution of our spectrum). For comparison, we also draw the same distribution for a random realization of a spectrum having the same resolution and the same average noise as the real data, but with zero average flux. One should actually do this pixel-to pixel using the individual pixel errors (see Fan et al. 2001c) but such a detailed analysis is beyond the scope of this paper. In any case the "random" line is clearly above the data, implying that the observed spectrum has finite non-zero average flux in this wavelength region and cannot be solely due to the noise alone. McDonald & Miralda-Escudé (2001) present the detailed flux distribution from simulated spectra at slightly lower absorption redshift. Their prediction could be easily compared with these data. For example at z_{abs} =5.2 they predict that only 3% of the spectrum should have a flux higher than 50% of the continuum, and less than 0.5% should have a flux greater than 75% of the continuum. Simulations show that because the IGM is highly clumpy, most of the flux that we observe is transmitted from a few of the most underdense voids, consistent with what is seen here (see the detailed discussion in Fan et al. 2001c).

3.3. *The proximity effect*

The spectrum shows excess transmitted flux immediately blueward of the Lyα line, as well as several absorption lines. This is due to the fact that luminous quasars such as SDSS 1030+0524 ionize the surrounding regions and create HII regions of radius several Mpc, the so-called "proximity" effect (e.g. Carswell et al. 1982). The transmitted flux extends over about 100 Å blueward (i.e., to 8750 Å) of the Lyα emission peak at 8850 Å. This corresponds to a distance of about $23h^{-1}$ Mpc comoving, or a proper size of D_{obs} =3.1h^{-1} Mpc at the epoch z=6.28.

The size of the HII region associated with the quasar depends on the luminosity and lifetime of the quasar and the clumpiness of the gas near the quasar. As pointed out by Madau & Rees (2000), if the lifetime of the quasar is shorter than the recombination time recombination can be neglected, and the evolution of the HII region can be decoupled from the expansion of the universe. This holds at z=6.28 on Mpc scales if the clumpiness factor C is less than ∼10. The photons will travel freely in the highly ionized bubble and will be absorbed in a transition layer (I-front). This I-front will initially expand at a velocity very close to the speed of light, but the Lyα and continuum photons from the quasar cannot "catch up" with the boundary of the HII region until its expansion speed slows down (Cen & Haiman 2000), when it first begins to be limited by the number of ionizing photons.
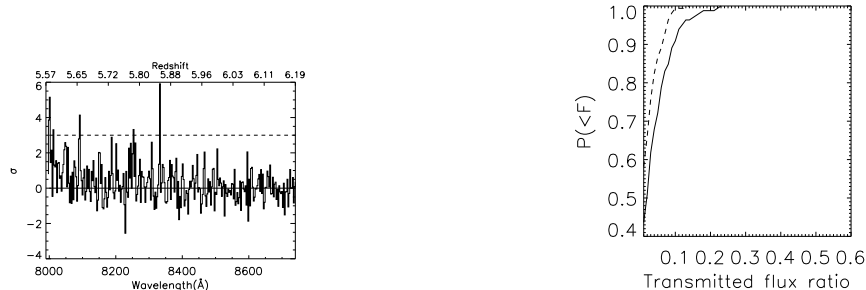
Fig. 4.— Left: an enlargement of the region between 8000 Å and 8750 Å, plotted in terms of significance, i.e. at each pixel the observed spectrum has been divided by the error array. The dashed line represent the 3 σ level: clearly there are no peaks beyond 8400 Å. The spectrum was binned to the resolution ($\sim$ 3 Å). Right: the cumulative distribution of the transmitted flux ratio for the spectrum in the 8000-8400 Å region. The spectrum has been rebinned to the resolution $\sim$ 3Å/pixel. The dashed line indicates the same distribution for a random realization of a spectrum with zero average flux and the same average noise of the real data.

In practise, the volume of ionized region that we observe will be proportional to the number of Lyman-continuum photons that are emitted over the source lifetime. In a homogeneous medium we can write:

$$V_I = \frac{4}{3}\pi D_I^3 = \frac{t_Q \dot{N}_{ph}}{n_H f}$$

where $\dot{N}_{ph}$ is the photo-ionization rate, and n_H is the mean hydrogen density within D_I. Following the papers cited, and in particular Cen & Haiman 2000, we use the mean hydrogen density given by $n_H = 1.6 \times 10^{-7}(1 + z)^3(\Omega_b h^2/0.02)$ cm^{-3}. However as we remarked earlier, luminous quasars probably reside in significantly overdense regions: the unknown bias factor will contribute to the uncertainty of the proximity effect region. In the equation above, f is the fraction of neutral hydrogen present when the quasar switches on. From the observations the only constraint we have is that $f \geq 0.01$ at $z \sim 6$ (Fan et al. 2001c). Simulations (e.g. Gnedin 2000) indicate that the ionizing fraction could be $f = 0.1$ or more at $z = 6.28$. Taking the quasar luminosity as $L_\nu \propto \nu^{-\alpha}$, we derive a total photo-ionization rate for the quasar of $\dot{N}_{ph} = 2/\alpha \times 10^{57}$ s^{-1}. Therefore the quasar must have been on for $t_Q \sim 1.3 f\alpha \times 10^7$ yrs. This is the total time during which the quasar has been emitting ionizing photons, and not necessarily the time elapsed since it first turned on. The derived time is of the same order as the e-folding timescale for a black hole accreting with 0.1 efficiency of the Eddington luminosity of 4×10^7 yr (Salpeter 1964).

Note that t_Q is shorter than the light-crossing time of the HII region ($\sim 1.5 \times 10^7$ yrs). The reason is that photons along the line of sight have been emitted at different redshift and therefore at different lookback times. Therefore it is not correct to set a minimum lifetime of the quasar by saying that those photons that are ionizing the edges of the HII region needed a certain time to propagate there, travelling at the speed c, since they could have been emitted at a later time. The light-travel argument would only be right if we could observe the HII region seen around the quasar in the plane of the sky.

The above calculation does not take into account other effects such as the presence of Lyman limit systems near the quasar, which would completely absorb the flux and produce a cutoff in the spectrum. In fact such a single overdense (and therefore neutral) cloud along the line of sight between the quasar and us is quite likely to exist close enough to the quasar to give a biased answer for the size of the ionized region (see Fan et al. 2001c). The presence of a Lyman limit system close to the quasar would lead to an underestimate of the quasar lifetime.

The transmitted flux profile blueward of the Lyα line also shows numerous absorption features which are produced by the density fluctuations of the medium around the quasar but are not resolved in the present spectrum. Cen & Haiman (2000) show that much higher spectral resolution measurements (R$\sim 10^4$) of the blue side of Lyα in bright quasars would provide direct estimates of the density fluctuations of gas on small scales.

The proximity effect is one of the primary techniques used to estimate the photo-ionization rate of the IGM (e.g. Bajtlik, Duncan, & Ostriker 1988, Bechtold 1994), by determining the distance from the quasar at which the optical depth of the Lyα forest is half that in the Gunn-Peterson trough. However, in the case of our quasar, the ionizing background is dominated by the flux of the quasar itself, so the profile of the Lyα line is insensitive to the ionization state of the IGM.

4. METALLICITY IN THE TWO HIGHEST REDSHIFT QUASARS

The metallicity (Z) of the gas around high-redshift quasars contains important information on the enrichment history of the gas in the quasar environment, and probes the star formation that came before the epoch of the observations, possibly the first stars that formed in massive collapsed structures (e.g. Hamann & Ferland 1999). In particular, line ratios involving nitrogen are valuable tracers of chemical enrichment, since this element is selectively enhanced by secondary processing in stellar populations and its abundance increases roughly as Z^2.

There is increasing evidence from measurements of various line ratios that the metallicity of the broad line regions around quasars have solar or supersolar values even at redshifts higher than 4, implying that there are stars at that redshift with ages exceeding 1 Gyr (e.g. Elston et al. 1994, Thompson et al. 1999). Clearly, dating the first star formation becomes increasingly interesting at redshifts of 5 or beyond, as the age of the universe approaches the enrichment timescale itself. At redshifts 5.99 and 6.28 the universe is only 910 Myr and 860 Myr old respectively, in our adopted cosmology.
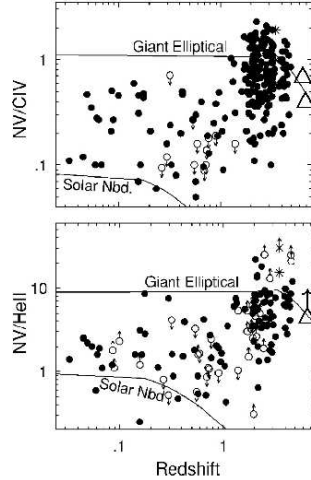
FIG. 5.— Measured NV/CIV and NV/HeII line ratios versus redshift for quasars up to z∼ 4 reproduced from Hamann and Ferland (1999) and with the addition of the new values measured for the 2 highest redshift quasars (represented as triangles).

From our spectrum of the z=6.28 quasar, we are able to measure the characteristics of the Lyα, NV and CIV emission lines, which are reported in Table 1. We do not detect HeII, but we can set an upper limit based on the S/N of the continuum. For the redshift 5.99 quasar, we combine our measurement of the CIV line with the Lyα and NV values derived by Becker et al. (2001). The derived line ratios for the redshift 6.28 quasar are NV/CIV= 0.35, slightly lower but consistent with that previously reported by Becker et al. (2001), and NV/HeII > 4.3. For the redshift 5.99 quasar, the restframe EW of the CIV line is 37 ± 6 Å; using the reported restframe EW of NV from Becker et al. (EW=17.9 Å), we derive for this object a NV/CIV ratio of 0.67. Note that in all cases we have derived the line ratios using the EW of each line and assuming that the continuum has the form of a power law with $f_\nu \propto \nu^{-\alpha}$ and $\alpha = 0.5$ as previously used.

In Figure 5 we show the measured values for NV/HeII and NV/CIV, in a plot of line ratios versus redshift reproduced from Hamann & Ferland (1999), which includes measured values for quasars at different redshifts. The line ratios of z∼6 quasars appear fully consistent with those at redshift between 2 and 4, indicating little evolution in the abundances, and hence metallicities, of quasar environments. However metallicity might be actually more a function of local density than of redshift (e.g. Cen & Ostriker 1999); we also know that metallicity scales with quasar luminosity, and since the two quasars are the brightest objects at that redshift, we might argue that the most luminous objects at z∼ 6 have lower metallicity than their counterparts at z∼ 4. Clearly more statistics are needed to determine whether we are starting to see a decline in metallicity as compared to z∼4.

Figure 5 also shows the predictions based on the Hamann & Ferland (1993,1999) chemical evolution models. The models that best reproduce the observed ratios for the two z≥ 6 quasars are those of "Giant Elliptical" nitrogen enrichment; these models involve short star formation timescales (0.5 Gyr) and IMF favoring high mass stars. The solar neighborhood models severely under-predict the two line ratios (NV/HeII and NV/CIV). If we plot the

observed line ratios into Figure 6 of Hamann & Ferland (1999), we derive a metallicity of roughly 7-8 $Z_\odot$ for our two quasars. We emphasize that the actual value of the metallicity is somewhat uncertain, due to the uncertainty in deriving reliable abundances from the emission line ratios: e.g. varying the shape of the EUV continuum, varying the mix of ionization parameter and column density in the radiating regions, and allowing for scattering contributions to NV 1240 (e.g. Krolik & Voit, 1998) can all perturb the relative line strengths without indicating anything about the abundances. However the main result is that the observed ratios definitely require $Z \geq Z_\odot$. Note that metallicity can be derived self-consistently from the two separate line ratios only if N$\propto Z^2$.

From the models of Hamann & Ferland (1993) we see that the minimum time needed for a stellar population to achieve the observed metallicity in any of their models is about 300 Myr. In the assumed cosmology the implied redshift of star formation is z∼8.7, an epoch when the universe was about ∼560 Myr old. Even if the quasar environments had only solar metallicity, the time required for any stellar population to reach such a metallicity would be on the order of 100 Myrs or more, implying that the star formation must have begun well before the observed quasar activity. Again these results are effected by the uncertainties of the models outlined above: other elements and in particular Fe, might provide better "clocks" for constraining the age of quasars and the epoch of first star formation. Fe has a large delayed contribution from type Ia supernovae, with a predicted time delay of about 1 Gyr after the initial starburst (Greggio & Renzini 1983, Matteucci & Greggio 1986) which does not depend on other parameters such as star formation rate etc. Therefore the ratio of Fe to α elements such as Mg is an absolute clock for constraining the ages of star forming regions. This will be pursued with follow-up observations in K-band where there are interesting features such as the broad FeIIλ2960 and the MgIIλ2798 lines.

5. CONCLUSION

We have presented new optical and near-IR spectroscopic observations of the two most distant quasars known,

at redshifts 6.28 and 6.0. We have confirmed the presence of a complete GP trough in the highest redshift object, derived new limits on the transmitted flux and optical depth in this region, and analyzed the characteristics of the flux emission in the region. In Fan et al. (2001c) we use semi-analytic models to study the evolution of the ionizing background and the epoch of reionization from the $z \sim 6$ quasars.

From the optical and near-IR spectra, we have estimated the metallicities of these early quasar environments, finding supersolar values for both objects. These high metallicities imply that the first stars around the quasars must have formed at least a few hundreds of Mpc prior to the observation, i.e. at redshifts higher than 8. Follow-up observations of other metal emission lines will help us to better constrain the ages of the star forming regions.

REFERENCES

Anderson, S. F. et al. 2001, AJ, 122, 503
Barkana, R. 2001 astro-ph/0108431
Bajtlik, S., Duncan, R. C., & Ostriker, J. P. 1988, ApJ, 327, 570
Becker, R. H. et al. 2001 AJ, 122, 2850
Bechtold, J. 1994, ApJS, 91, 1
Bertin, E. & Arnouts, S. 1996, A&AS, 117, 393
Carswell, R.F., Whelan, J.A.J., Smith, M.G., Boksenberg, A., & Tytler, D. 1982, MNRAS, 198, 91
Cen, R. & Haiman, Z. 2000, ApJ, 542, L75
Cen, R. & McDonald, P. , AJ submitted astro-ph/0110306
Cen, R. & Ostriker, J. P. 1999, ApJ, 519, L109
Djorgovski, S. G., Castro, S., Stern, D., & Mahabal, A. A. 2001, ApJ, 560, L5
Efstathiou, G. & Rees, M. J. 1988, MNRAS, 230, 5P
Elston, R., Thompson, K. L., & Hill, G. J. 1994, Nature, 367, 250
Fan, X. et al. 2000, AJ, 120, 1167
Fan, X. et al. 2001a, AJ, 121, 31
——, 2001b, AJ, 122, 2833
——, 2001c, AJ, accepted, astro-ph/0111184
Gnedin, N. Y. 2000, ApJ, 542, 535
Greggio, L. & Renzini, A. 1983, A&A, 118, 217
Gunn, J. E., & Peterson, B. A. 1965, ApJ, 142, 1633
Haiman, Z. ;. & Loeb, A. 1999, ApJ, 519, 479
Hamann, F. & Ferland, G. 1999, ARA&A, 37, 487
Hamann, F. & Ferland, G. 1993, ApJ, 418, 11

Hamuy, M., Walker, A. R., Suntzeff, N. B., Gigoux, P., Heathcote, S. R., & Phillips, M. M. 1992, PASP, 104, 533
Kauffmann, G. & Haehnelt, M. 2000, MNRAS, 311, 576
Krauss, L., & Turner, M. 1995, Gen. Rel. Grav., 27,1137
Krolik, J. H. & Voit, G. M. 1998, ApJ, 497, L5
Laor, A., Bahcall, J. N., Jannuzi, B. T., Schneider, D. P., & Green, R. F. 1995, ApJS, 99, 1
Lidz, A. et al. ApJ submitted astro-ph/0111346
Loeb, A. & Barkana, R. 2001, ARA&A, 39, 19
Madau, P. & Rees, M. J. 2000, ApJ, 542, L69
Matteucci, F. & Greggio, L. 1986, A&A, 154, 279
McDonald, P. & Miralda-Escudé, J. 2001, ApJ, 549, L11
Miralda-Escudé, J., Haehnelt, M., & Rees, M. J. 2000, ApJ, 530, 1
Nusser, A. & Silk, J. 1993, ApJ, 411, L1
Oke, J. B. & Korycansky, D. G. 1982, ApJ, 255, 11
Ostriker, J. P., & Steinhardt, P. 1995, Nature, 377, 600
Salpeter, E. E. 1964, ApJ, 140, 796
Scheuer, P. A. G., 1965, Nature, 207, 963
Schneider, D. P. et al. 2001, AJ, 121, 1232
Shklovsky, I.S., 1964, Astron. Zh. 41, 408
Stoughton, C. et al. 2002, AJ, 123, 485
Thompson, K. L., Hill, G. J., & Elston, R. 1999, ApJ, 515, 487
Vanden Berk, D. E. et al. 2001, AJ, 122, 549
York, D. G. et al. 2000, AJ, 120, 1579
Zheng, W. et al. 2000, AJ, 120, 1607

TABLE 1
EMISSION LINE PROPERTIES.

Line	redshift	flux 10^{-15}erg s^{-1} cm^{-2}	FWHM km s^{-1}	EW[a] Å
Lyα	–	2.70	4000±400	41.9±4
NV	6.29 ±0.01	0.86	2400±260	14.3±4
CIV	6.27 ±0.02	3.2	5600±400	42.5±5
HeII	–	<0.20	—	< 3.3

[a]Restframe EW

TABLE 2
CHARACTERISTICS OF EMISSION FEATURES IN THE 8000-8400 Å RANGE OF THE SPECTRUM.

num	λ_0 Å	Flux 10^{-17}erg s^{-1} cm^{-2}	Width(1σ) Å
1	8000.4	1.59	8.2
2	8006.3	0.43	2.
3	8012.7	0.92	4.8
4	8047.1	1.02	7.5
5	8091.4	1.12	5.4
6	8150.6	0.49	4.1
7	8253.1	0.67	4.8
8	8332.9	1.02	4.8